



A comparison of deformation, microstructure, mechanical properties and formability of SUS436L stainless steel in tandem and reversible cold rolling processes

Wen-tao Wang¹ · Jiao Zhang¹ · Feng-li Sui¹ · Zhi-xia Zhang² · Hong-yun Bi²

Received: 8 May 2018 / Revised: 5 September 2018 / Accepted: 7 September 2018 / Published online: 21 September 2018
© China Iron and Steel Research Institute Group 2018

Abstract

A comparison was made for the deformation, microstructure, mechanical properties and formability of SUS436L stainless steel in tandem and reversible cold rolling processes. At first, the thermophysical parameters and stress–strain curves of SUS436L steel were measured in temperature range of 293–573 K and a flow stress model was regressed from the data of these curves. An analytical model based on the elasto-plastic finite element method was then established to simulate the tandem and the reversible cold rolling processes of SUS436L stainless steel strip where the flow stress model was introduced. The difference in shear strain distribution, microstructure, mechanical properties and formability of SUS436L steel strip in the two rolling processes was analyzed. The results showed that the larger shear strain, the enhanced intensity of γ fiber texture and the excellent formability of the strip can be easily obtained in the tandem rolling process with the larger work roll rather than the reversible rolling process with the smaller work roll.

Keywords SUS436L stainless steel · Cold rolling · Finite element method · Shear deformation · γ fiber texture

1 Introduction

The share of ferritic stainless steel in the stainless steel family presents a rising trend owing to the scarcity of nickel resource [1, 2]. In order to obtain the similar, even more superior performance to the austenitic stainless steel, technical measures such as purification [3], micro-alloying [4, 5] and optimization of rolling process [6, 7] have been applied in the strip manufacturing of the ferritic stainless steel. In addition to the above measures, the selection of rolling equipment is still the important way to obtain the excellent mechanical properties.

The ferritic stainless steels have been widely used in kitchen wares, electrical appliances, architectural and automobile industries because of their high thermal

conductivity, perfect oxidation and corrosion resistance [8–10]. In contrast to the austenitic stainless steel, the ferritic stainless steel, especially 400 series of ferritic stainless steel, has the higher yield stress and lower total elongation in cold rolling process [11–13]. According to the formula of Stone [14], the reversible rolling (RR) process using the work rolls with small diameter (60–80 mm) is the traditional one for cold rolling of the ferritic stainless steels. However, the rolling yield and the production efficiency are both low in such rolling process. In order to solve these problems, the tandem rolling (TR) way will be widely used in the cold rolling strip production for the ferritic stainless steels with the improvement of the performance for the rolling mill. The relation between the shear deformation and the microstructure distribution along the through-thickness has been analyzed by Ma et al. [15] in the hot rolling process of a high-Mn non-magnetic steel. According to the viewpoint of Gao et al. [7], the recrystallized grain will preferably nucleate in the shear bands formed in the lower-temperature rolling process for 17% Cr ferritic stainless steel. Undoubtedly, it is of great importance to study the difference in the shear deformation in rolling process, the microstructure, mechanical

✉ Feng-li Sui
suiflahut@126.com

¹ School of Metallurgical Engineering, Anhui University of Technology, Ma'anshan 243002, Anhui, China

² State Key Laboratory of Development and Application Technology of Automobile Steels, Baowu Steel Group Co., Ltd., Shanghai 201900, China

properties and formability of the final strip of the ferritic stainless steels in the two rolling processes. Recently, the shear stress distribution of cold rolled strip in rolling process has been analyzed based on the finite element (FE) method [16], but there is no report on the distribution of shear strain for the cold rolled strip in rolling process.

In this study, a typical ferritic stainless steel SUS436L was used in cold rolling process, and rolling processes such as TR in five-stand rolling mill and RR in the Sendzimir mill were chosen to be analyzed. At the same time, the distribution of the shear strain along the longitudinal cross section of the cold rolled strip was analyzed based on elasto-plastic FE method. At last, the difference in shear strain distribution, microstructure, mechanical properties and formability of SUS436L steel strip in the cold TR and RR processes was obtained and analyzed.

2 Thermophysical parameters and flow stress model

The ferritic stainless steel SUS436L with the following composition (in wt.%) was used in this study: C 0.011, Si 0.42, Mn 0.25, Cr 17.45, Mo 0.88, Ti 0.23, Nb 0.014, N 0.008, P 0.025, S 0.002 and Fe balance. The density (ρ), specific heat capacity (c), thermal expansion coefficient (α), thermal conductivity (λ) and elastic modulus (E) of SUS436L adopted in this work were experimentally obtained and are presented in Table 1.

The uniaxial compression experiments were conducted on Gleeble-3500 thermomechanical simulator at 293, 373, 473 and 573 K. Since the dynamic recrystallization cannot occur in the cold rolling process and the dynamic recovery is not as enough as it is in the hot deformation process [17], the influence of the strain rate on the flow stress can be omitted and the strain rate was chosen to be 0.1 s^{-1} as the deformation strain rate. The specimens of $\phi 8 \text{ mm} \times 12 \text{ mm}$ [18] used in the experiments were machined from the hot rolled billet of SUS436L steel. The experimentally determined stress-strain curves are shown in Fig. 1, and the flow stress model was regressed from the data of these curves, as shown in Eq. (1).

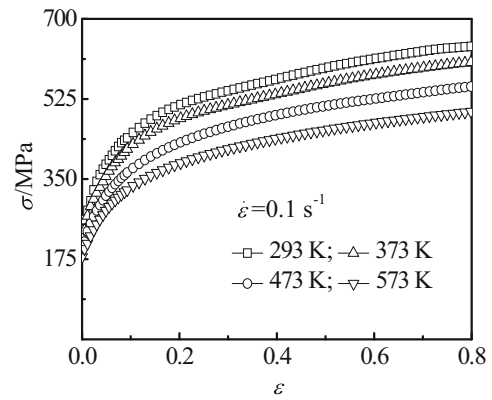


Fig. 1 True stress-strain curves of SUS436L steel

$$\sigma = 240 \exp\left(1.1027 - \frac{0.9548T}{1000}\right) \left[1.0887\left(\frac{\varepsilon + 0.0105}{0.3}\right)^{0.2660} - 0.0887\left(\frac{\varepsilon + 0.0105}{0.3}\right)\right] \quad (1)$$

where σ is the equivalent stress, MPa; ε is the equivalent strain and T is the deformation temperature, K.

The comparison between the regressed stress values (σ_{reg}) based on calculation from Eq. (1) and the experimentally measured values (σ_{tes}) is displayed in Fig. 2. The relative deviation of the regressed stress values to the tested ones is less than 7.0%, and the regressed values with the relative deviation no more than 3.0% to the tested ones have a high percentage of 89.64%.

3 Establishment of FE model

The strip billet with thickness of 4.5 mm are tandem cold rolled in five-stand rolling mill with the work roll in a diameter of 405 mm and reversible cold rolled in the Sendzimir mill with the work roll in a diameter of 60 mm, respectively. Due to the large ratio of width to thickness of the strip billet, the width spread can be omitted and a thermal-coupled two-dimensional model (in Fig. 3) was established based on the software Msc.MARC using the elasto-plastic FE method considering the elastic recovery

Table 1 Thermophysical parameters of SUS436L steel

$\rho/(\text{kg m}^{-3})$	E/GPa		α/K^{-1}		$\lambda_{(293-573 \text{ K})}/(\text{W m}^{-1} \text{ K}^{-1})$	$c_{(293-573 \text{ K})}/(\text{J kg}^{-1} \text{ K}^{-1})$
	293 K	473 K	293-473 K	473-573 K		
7.73×10^3	220	183	1.05×10^{-5}	1.15×10^{-5}	26.0	460

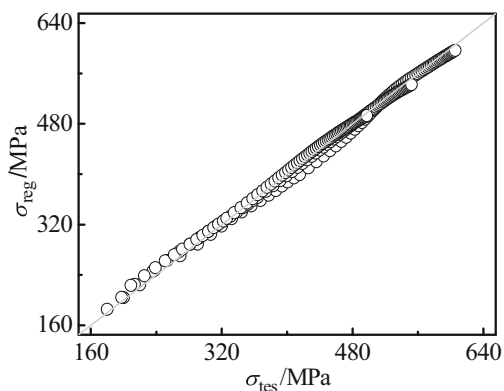


Fig. 2 Comparison of stresses between regressed and tested values

of the ferritic stainless steels and the conversion of plastic work to heat in cold rolling process. In this model, the strip billet with the half thickness and only a work roll are adopted considering the symmetry of the rolling process. The displacement constraint $U_y = 0$ in y direction is applied on the nodes in the symmetrical line in the midst of the billet, the tension forces T_f and T_b are separately exerted on the nodes in the head and the tail lines of the billet, and the angular velocity ω_u calculated by the rolling speed v for different rolling passes ($\omega_u = v/R$) is applied on the work rolls. Since the radius (R) of the work rolls is unchanged in the whole rolling process, 30 mm for the RR one and 202.5 mm for the TR one, a FE model with the single stand is adopted and the strip billet is cold rolled by the moving direction change for the billet and the position adjustment for the work roll in the rolling processes. The quadrilateral plane element (Quad 8) is used in FE analysis, and the thickness of that shell is set as 1 mm. The billet with stable length of 70 mm was meshed for different

element sizes of 0.75, 0.56, 0.45, 0.38, 0.32 and 0.28 mm. As a result, the half thickness and the length were divided into 3×90 , 4×125 , 5×155 , 6×184 , 7×218 and 8×250 units. The established FE models with 155 elements in the length and 5 elements in the half thickness for TR and RR in stable rolling process are separately shown in Fig. 3a, b.

4 Results and discussion

The final strip is 1.2 mm in thickness, and the different rolling passes are used in the practical rolling processes (shown in Table 2) according to the rolling capacity of the rolling mills. In Table 2, i is the different rolling pass and η is the reduction rate, %. According to the parameters in Table 2, the cold rolling processes for TR and RR are simulated by using the related FE models in Fig. 3.

The rolling forces (F_r) simulated for the first rolling pass changed with the time step (T_s) at different element sizes and the corresponding measured values of practical F_r for unit width of the billet in TR and RR are separately illustrated in Fig. 4a, b. As the element size is no more than 0.45, the simulated F_r tends to be constant in the stable rolling process and the simulated maximal values of F_r are in good agreement with the measured ones. For fast solution convenience and enough deformation stability, the element size of 0.45 mm (155 elements in the length and 5 elements in the half thickness) is adopted for the billet in the following FE analysis.

The maximal rolling forces (F_{max}) for each pass between the simulated and the measured values in the practical rolling process are compared and displayed in

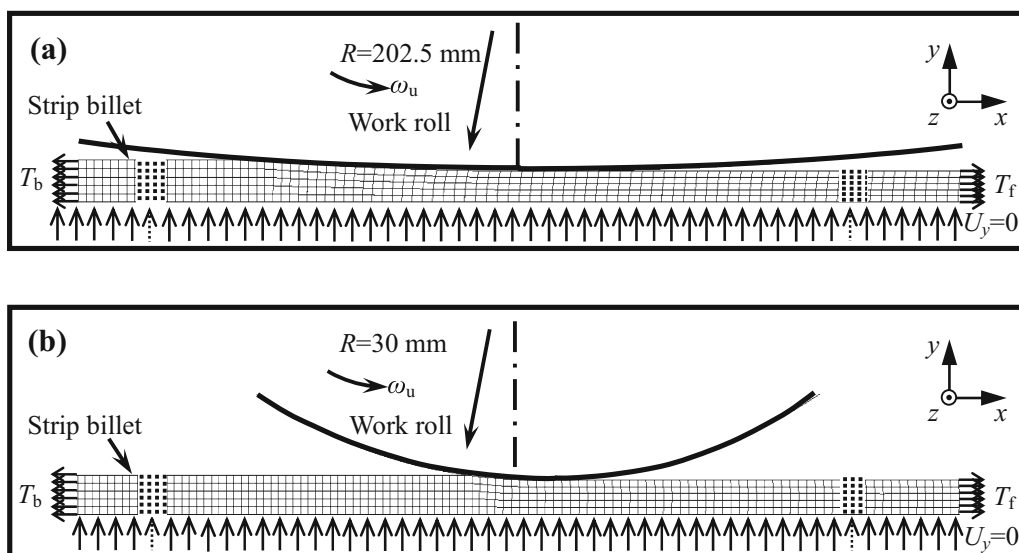


Fig. 3 FE model for stable cold rolling processes. a TR; b RR

Table 2 Parameters for cold rolling process

Rolling method	<i>i</i>	$\eta/\%$	$v/(\text{m min}^{-1})$	$T_b/(\text{kg mm}^{-1})$	$T_f/(\text{kg mm}^{-1})$
RR	1	10.02	225	4.80	40.00
	2	12.50	225	36.00	40.00
	3	15.71	225	36.80	37.60
	4	16.27	370	34.40	35.20
	5	15.46	382	27.20	28.80
	6	14.70	391	24.00	24.80
	7	13.92	392	21.60	22.40
	8	13.17	390	21.60	22.40
	9	10.96	290	20.00	20.80
TR	1	25.29	178	26.54	26.54
	2	27.25	245	26.54	20.57
	3	22.39	316	20.57	15.90
	4	19.57	393	15.90	12.05
	5	21.40	500	12.05	8.85

Fig. 5a, b. Obviously, the measured maximal rolling forces are larger than the simulated ones, but there is no significant difference between them. In other words, the simulated results are in good agreement with the measured ones.

4.1 Shear deformation of cold rolled strips by FE method

The distribution of the shear strain along the longitudinal cross section of the cold rolled strip for the first and the last passes in the five-pass TR process is shown in Fig. 6, and that for the first and the last passes in the nine-pass RR process is shown in Fig. 7. In Figs. 6 and 7, it can be seen that the shear strain distribution is homogeneous along the rolling direction, but inhomogeneous along the thickness direction. In both rolling processes, the larger shear strain gradient is mainly located in the surface of the final strip and the steep dropping band of shear strain is formed, while the band of the final strip for TR process is slightly higher than that for RR process. Except for the steep dropping band of shear strain, most area along the longitudinal section of the final strip is occupied by the uniform shear strain, 0.01222 for TR process (Fig. 6b) and 0.00111 for RR process (Fig. 7b). Obviously, the larger distributed shear strain can be obtained for the final strip in TR process with the larger roll diameter and the larger single-pass reduction. According to the viewpoints of Inoue et al. [19], the larger shear strain is beneficial to the grain refinement.

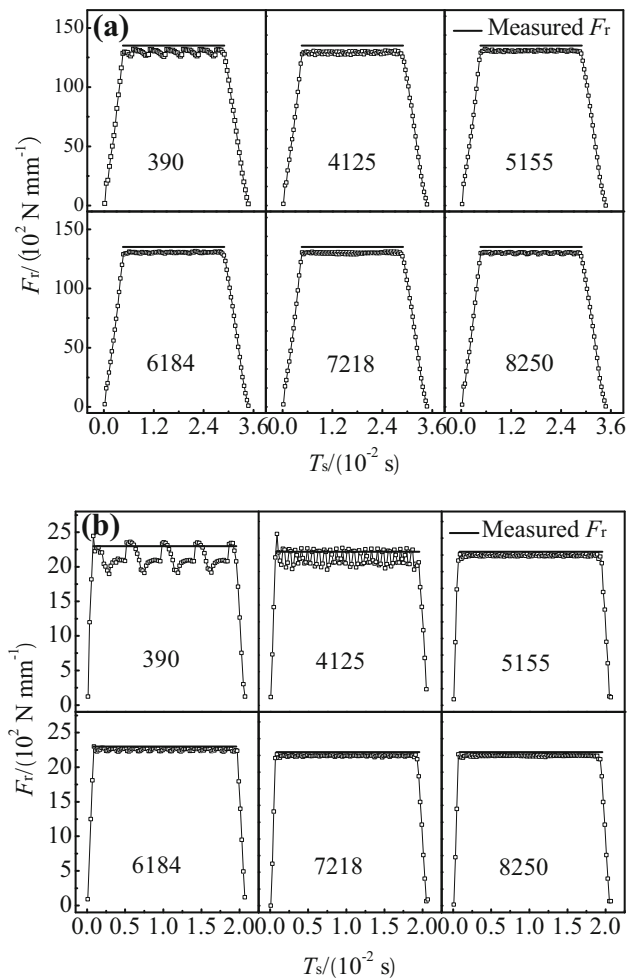


Fig. 4 Simulated rolling forces for different element sizes and measured maximal rolling force for first-pass rolling process. **a** TR; **b** RR

4.2 Microstructure, mechanical properties and formability of cold rolled and annealed strips

The optical micrographs for the final cold rolled and annealed strips with the thickness of 1.2 mm in the TR and RR processes are displayed in Fig. 8a, b, respectively. The homogeneously distributed grain with grain size of 31.5 μm has been obtained in TR process, while the grain obtained in the RR process is inhomogeneously distributed and the average grain size of which is about 45.0 μm . Obviously, the former rolling method is beneficial to the grain refinement and homogeneous distribution in annealing process by using the work roll with large diameter.

Formability is of importance for the ferritic stainless steel in the further cold forming process and is closely related to γ fiber texture recrystallized ($\langle 111 \rangle // \text{ND}$) [20, 21]. The intensity of γ fiber texture for the cold rolled and annealed strips has been analyzed by electron

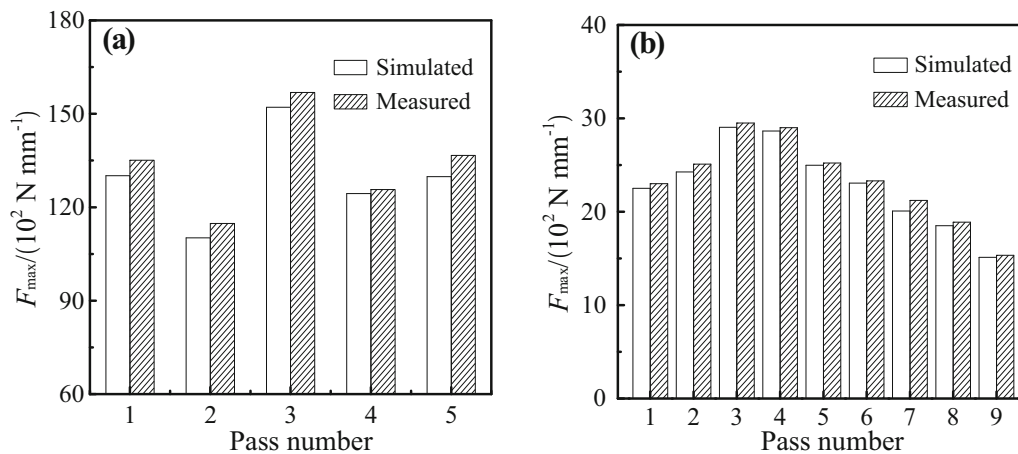


Fig. 5 Comparison of maximal rolling force in TR (a) and RR (b) between simulated and measured values

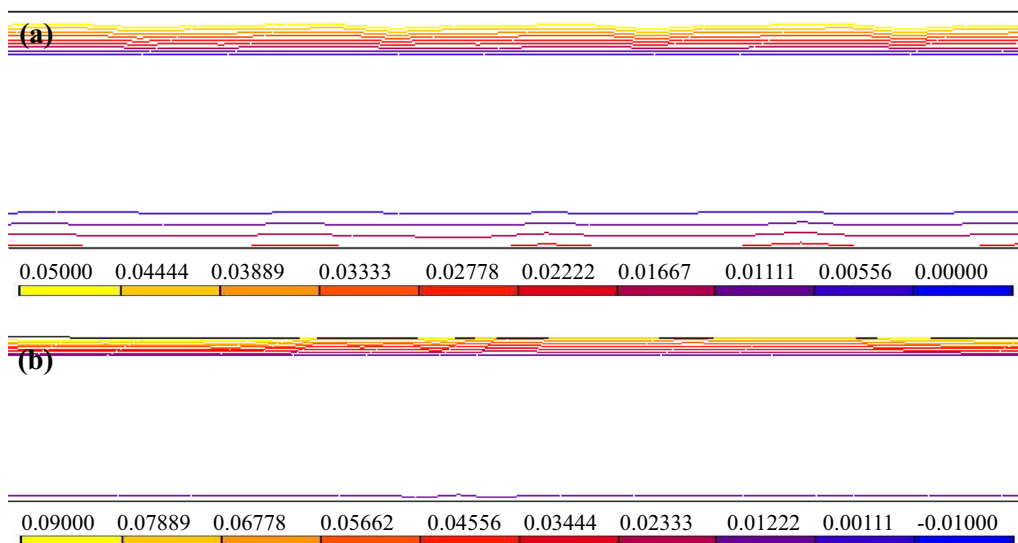


Fig. 6 Distribution of shear strain in longitudinal section of cold rolled strip in TR process

backscatter diffraction. The orientation distribution maps in the longitudinal cross section of the cold rolled strips in TR and RR processes are separately shown in Fig. 9a, b, and those of the annealed strips are shown in Fig. 10a, b. Orientation distribution function (ODF) maps for the whole thickness of the cold rolled strips in TR and RR processes are shown in Fig. 11a, b, and those of the annealed strips in Fig. 12a, b. The corresponding inverse pole figures are displayed in Fig. 13a, b for the cold rolled strips, and in Fig. 14a, b for the annealed strips.

From Figs. 11 and 12, α and γ textures form in the normal direction for the cold rolled strips and only γ texture exists in the annealed strips. The same phenomenon has been found by Gao et al. [22] for a ultra-purified ferritic stainless steel. The significant change in ODFs for the strip from the cold rolled state to the annealed one is α texture transforming to γ one; as a result, the intensity of γ texture

is enhanced. As $\phi_2 = 45^\circ$, it can be seen γ texture has higher intensity in TR process than that in RR process not only for the cold rolled strip but also for the annealed strip. The further analysis on the inverse figures indicates the intensity of γ fiber texture of the cold rolled strip is enhanced from 6.19 to 6.50 after annealing for TR process, and that for RR process is enhanced from 4.95 to 5.15 by comparing Fig. 13 with Fig. 14. Compared to RR process, TR process is the better way for the intensification of γ fiber texture since the work roll with the large diameter can provide enough deformation permeability and relatively larger shear strain is formed throughout the whole longitudinal cross section of the cold rolled strip.

The mechanical properties of the annealed strips for SUS436L steel such as the yield stress ($R_{p0.2}$), the tensile strength (R_m), the strain hardening exponent (n) as the engineering strain is from 5 to 15%, the plastic strain ratio

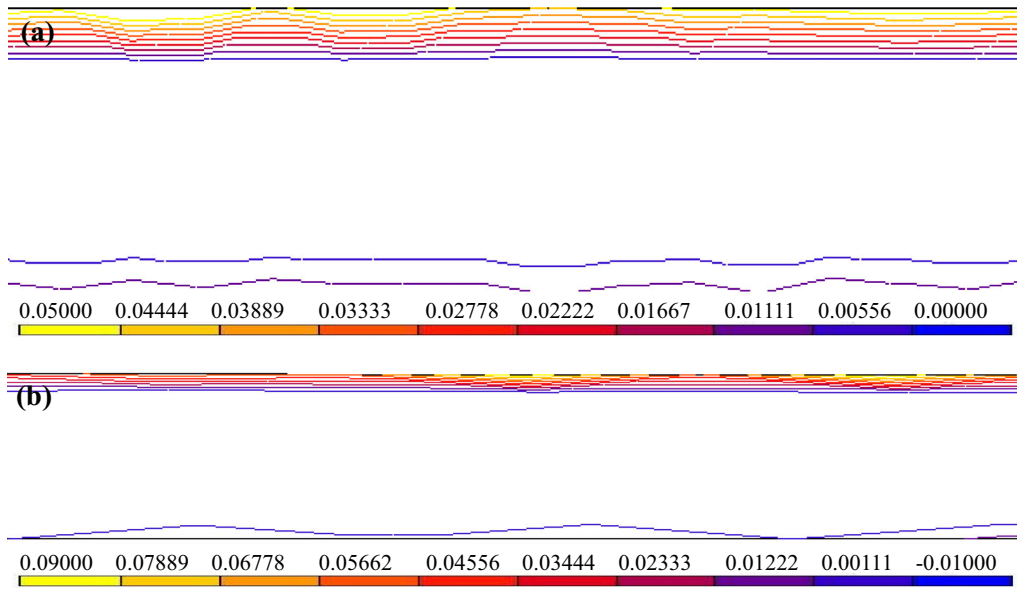


Fig. 7 Distribution of shear strain in longitudinal section of cold rolled strip in RR process

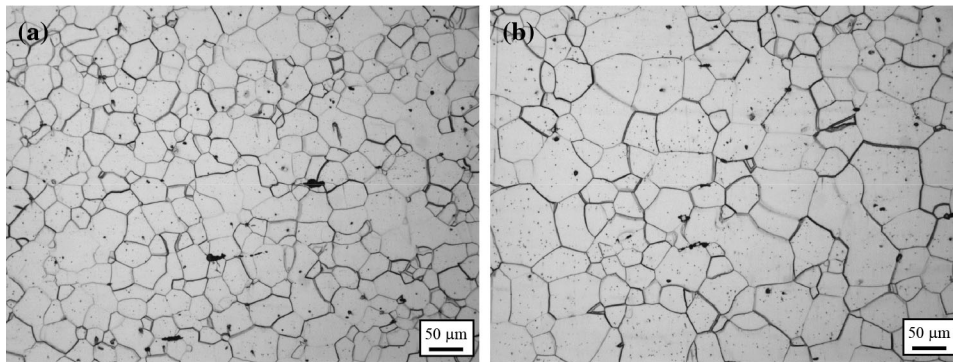


Fig. 8 Optical micrographs in longitudinal cross section of annealed strips with thickness of 1.2 mm in TR (a) and RR (b) processes

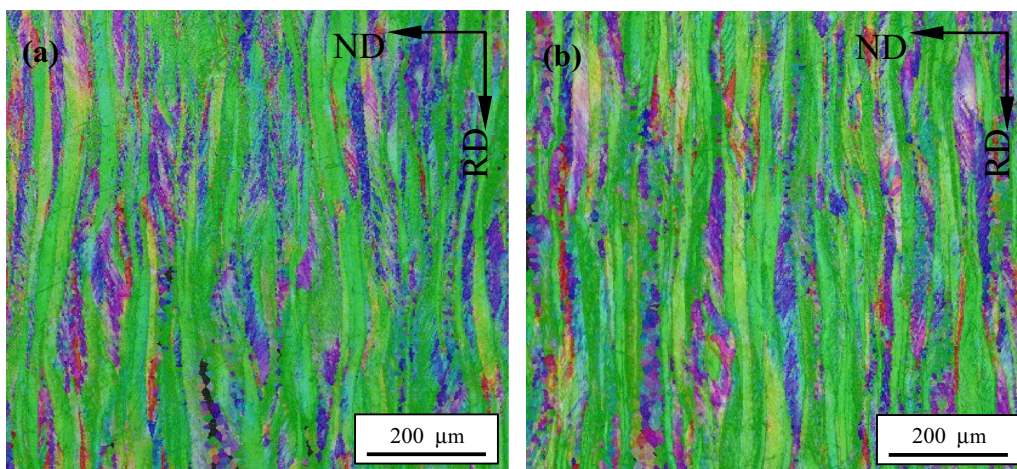


Fig. 9 Orientation distribution map in TD plane of cold rolled strips in TR (a) and RR (b) processes

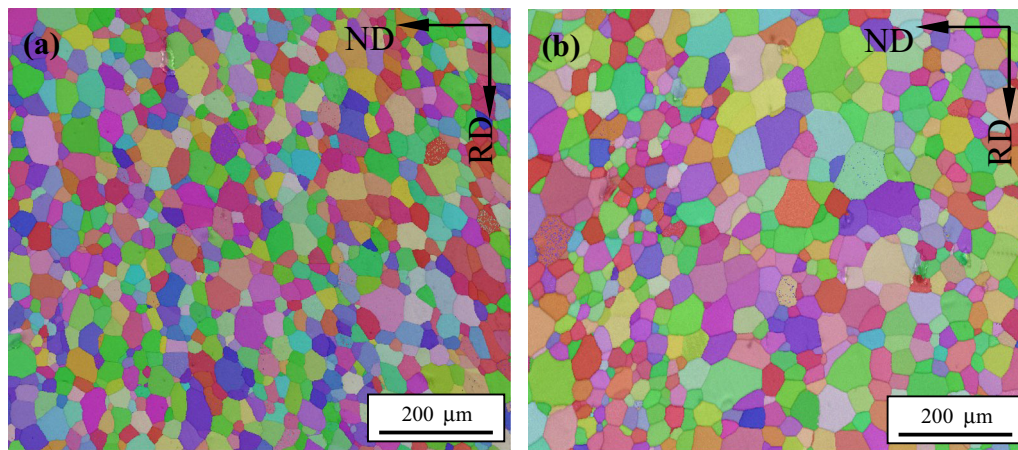


Fig. 10 Orientation distribution map in TD plane of annealed strips in TR (a) and RR (b) processes

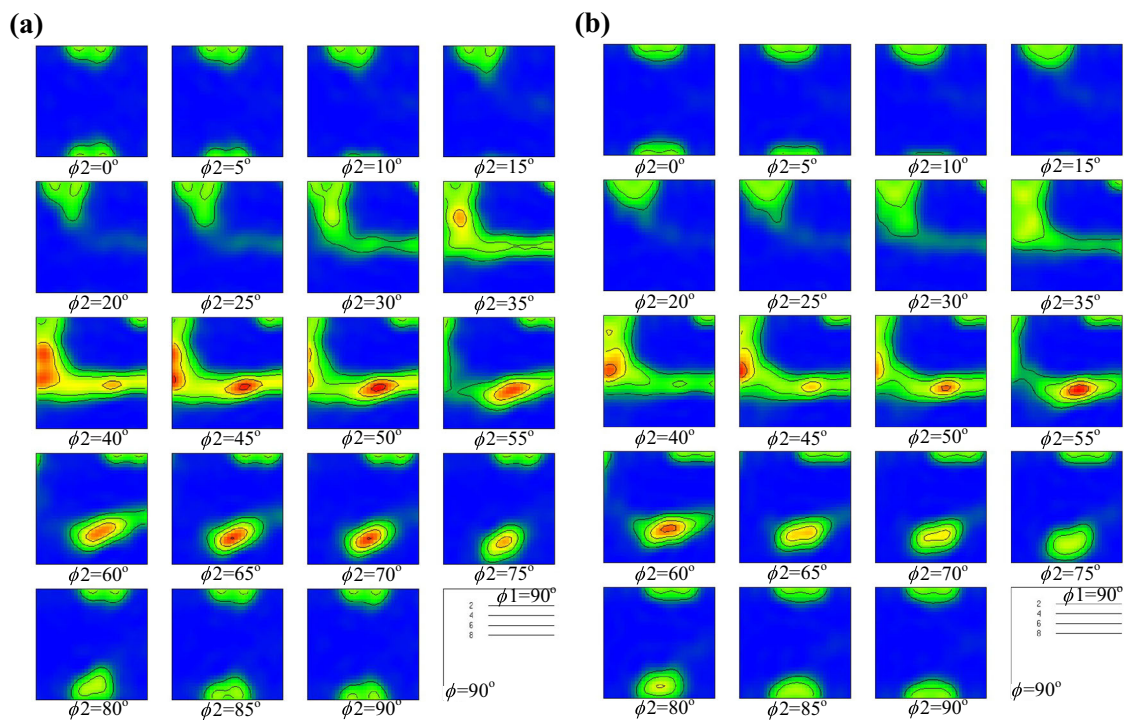


Fig. 11 ODF maps (ϕ_2 constant sections) for whole thickness of cold rolled strips in TR (a) and RR (b) processes

(r) as the engineering strain is 15%, the strain hardening coefficient (K) and the elongation rate (A) have been obtained by tensile tests in room temperature using the samples with width of 25 mm and gauge length of 50 mm fabricated from the annealed strips after the cold rolling processes, and the formability such as the Erichsen value (IE) and the limit drawing ratio (LDR) as well. The corresponding tested data are illustrated in Tables 3 and 4. The better formability and the excellent comprehensive mechanical properties are displayed in the annealed strip after TR process since the larger shear deformation existed

throughout the whole longitudinal cross section of the cold rolled strip and the finer grain size evenly distributed, especially the stronger γ fiber texture formed in the annealed strip.

5 Conclusions

1. A FE model has been built for shear deformation analysis in TR and RR cold rolling process. The results indicate that most area along the longitudinal section

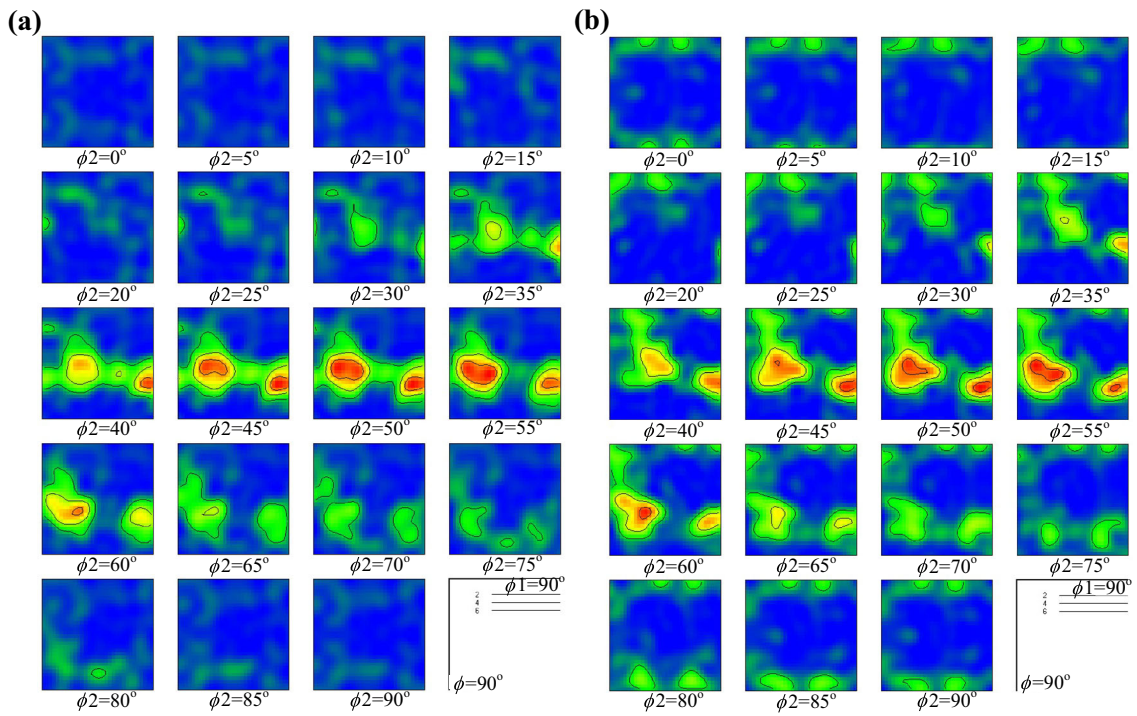


Fig. 12 ODF maps (ϕ_2 constant sections) for whole thickness of annealed strips in TR (a) and RR (b) processes

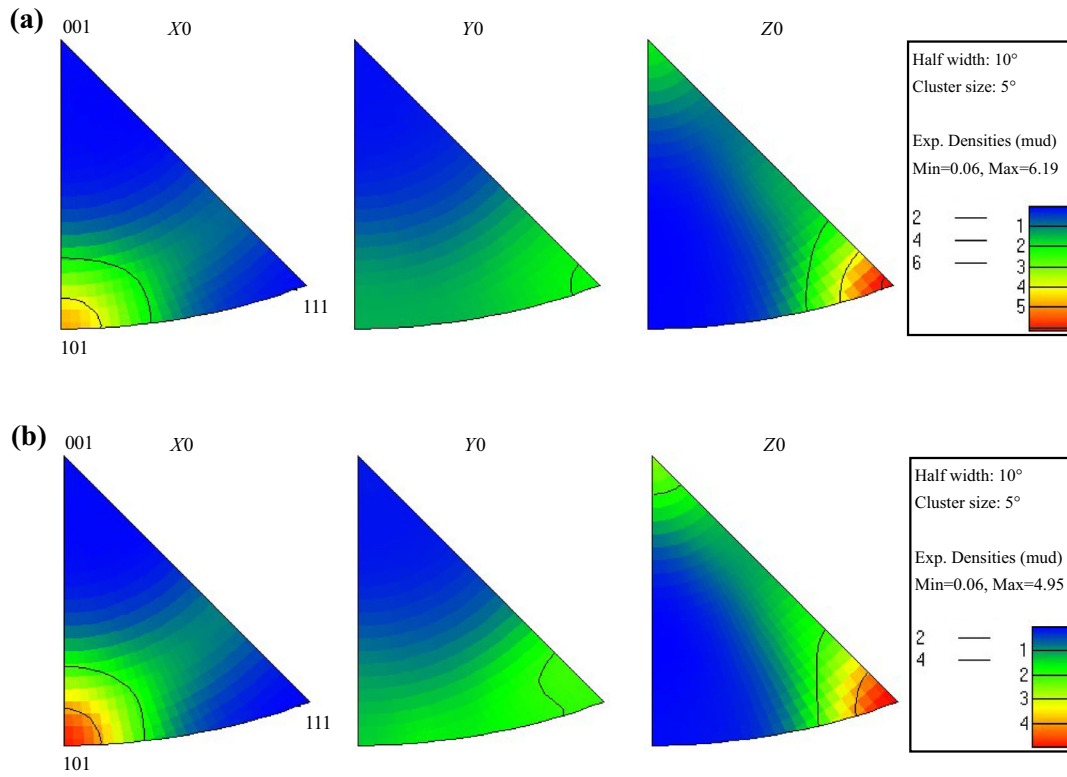


Fig. 13 Inverse figure of cold rolled strips in TR (a) and RR (b) processes

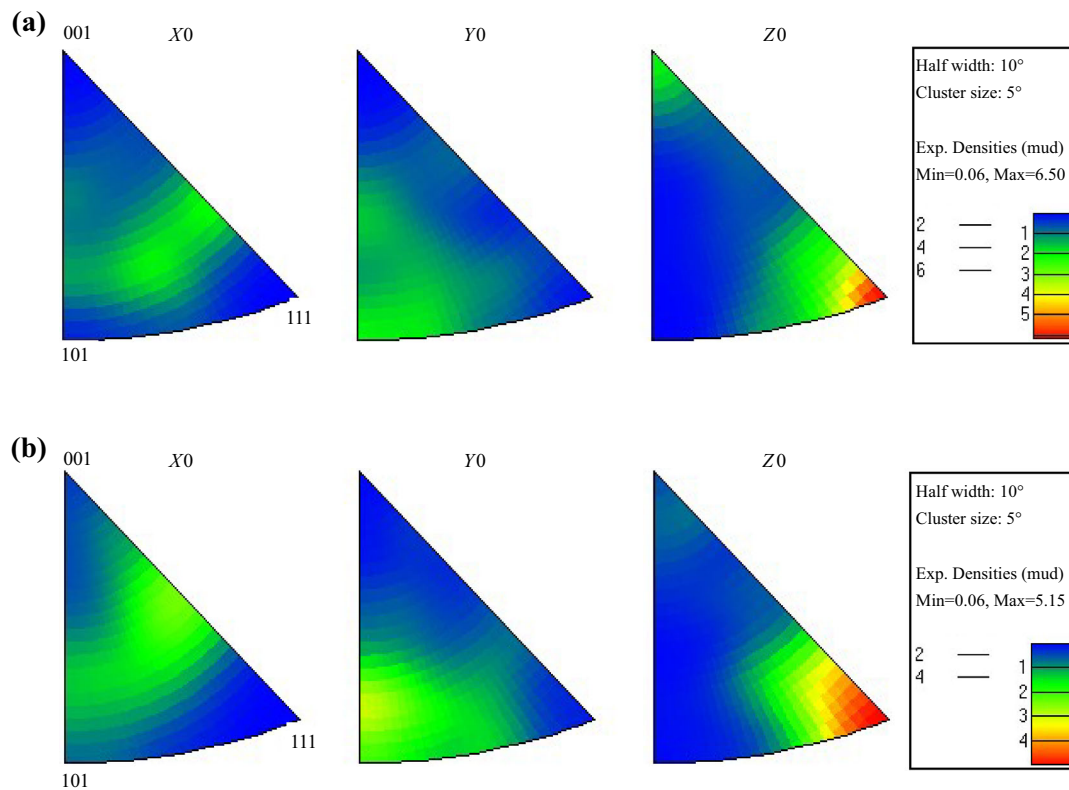


Fig. 14 Inverse figure of annealed strips with thickness of 1.2 mm in TR (a) and RR (b) processes

Table 3 Mechanical properties of SUS436L steel

Rolling mode	$R_{p0.2}$ /MPa	R_m /MPa	n	r	K	$A/\%$
TR	278.79	448.36	0.242	1.412	820	37.90
	279.59	446.46	0.243	1.411	825	38.04
	277.92	446.33	0.241	1.413	823	37.35
RR	269.63	436.15	0.236	1.237	790	37.72
	268.26	434.71	0.235	1.234	785	35.88
	268.45	436.59	0.236	1.237	788	36.58

Table 4 Formability of SUS436L steel

Rolling mode	IE/mm	LDR ($\phi 110$ mm)
TR	11.50	2.3
RR	11.34	2.2

of the final strip is occupied by the uniform shear strain, 0.01222 for TR process but 0.00111 for RR process, except for the steep dropping band of shear strain in the surfaces. This means that the cold rolled strip in the five-pass TR process has the more intensive shear deformation than that in the nine-pass RR

process along the longitudinal cross section with the same total reduction rate.

2. Analysis of microstructure, mechanical properties and formability for the cold rolled and annealed strips indicates that the smaller recrystallized grain size with higher intensity of γ fiber texture, more excellent mechanical properties and formability were obtained for the strip product cold rolled in the five-pass TR process.
3. The larger shear strain is beneficial to the grain refinement, γ fiber texture strengthening, mechanical property and formability improvement. Compared with RR cold rolling process, TR cold rolling process is a promising cold rolling way for the strip production of ferritic stainless steels.

Acknowledgements The authors are grateful for the joint financial support from the National Natural Science Foundation of China and Baowu Steel Group Co., Ltd. (Grant No. U1660205).

References

- [1] M.Y. Huh, J.H. Lee, S.H. Park, O. Engler, D. Raabe, *Steel Res. Int.* 76 (2005) 797–806.
- [2] H.T. Liu, Z.Y. Liu, G.D. Wang, *ISIJ Int.* 49 (2009) 890–896.

- [3] X.M. You, Z.H. Jiang, H.L. Li, *J. Iron Steel Res. Int.* 14 (2007) No. 4, 24–30.
- [4] Y.T. Shan, X.H. Luo, X.Q. Hu, S. Liu, *J. Mater. Sci. Technol.* 27 (2011) 352–358.
- [5] Y.T. Chiu, C.K. Lin, *J. Power Sources* 198 (2012) 149–157.
- [6] D. Raabe, K. Lücke, *Mater. Sci. Technol.* 9 (1993) 302–312.
- [7] F. Gao, Z.Y. Liu, H.T. Liu, G.D. Wang, *Mater. Charact.* 75 (2013) 93–100.
- [8] N. Fujita, K. Ohmura, M. Kikuchi, T. Suzuki, S. Funaki, I. Hiroshige, *Scripta Mater.* 35 (1996) 705–710.
- [9] L. Gardner, *Prog. Struct. Eng. Mater.* 7 (2005) 45–55.
- [10] J.K. Kim, Y.H. Kim, S.H. Uhm, J.S. Lee, K.Y. Kim, *Corros. Sci.* 51 (2009) 2716–2723.
- [11] X.F. Kang, *The ferritic stainless steel*, Metallurgical Industry Press, Beijing, 2012.
- [12] C. Zhang, Z.Y. Liu, Y. Xu, G.D. Wang, *J. Mater. Process. Technol.* 212 (2012) 2183–2192.
- [13] S.M. Kim, Y.S. Chun, S.Y. Won, Y.H. Kim, C.S. Lee, *Metall. Mater. Trans. A* 44 (2013) 1331–1339.
- [14] M.D. Stone, *Iron Steel Eng.* 30 (1953) 1–15.
- [15] B. Ma, C.S. Li, J.K. Wang, B. Cai, F.L. Sui, *Mater. Sci. Eng. A* 671 (2016) 190–197.
- [16] L. Hao, H.S. Di, D.Y. Gong, *J. Iron Steel Res. Int.* 20 (2013) No. 5, 34–37.
- [17] F. Gao, F.X. Yu, H.T. Liu, G.D. Wang, *J. Iron Steel Res. Int.* 22 (2015) 827–836.
- [18] F.L. Sui, Y. Zuo, J. Zhao, B.G. Ma, *Acta Metall. Sin. (Engl. Lett.)* 27 (2014) 494–500.
- [19] T. Inoue, S. Torizuka, K. Nagai, *Mater. Sci. Technol.* 18 (2002) 1007–1015.
- [20] Y. Yazawa, Y. Ozaki, Y. Kato, O. Furukimi, *JSAE Rev.* 24 (2003) 483–488.
- [21] J.I. Hamada, N. Ono, H. Inoue, *ISIJ Int.* 51 (2011) 1740–1748.
- [22] F. Gao, Z.Y. Liu, H.T. Liu, G.D. Wang, *J. Iron Steel Res. Int.* 20 (2013) No. 4, 31–38.